Electronic Supporting Information

3D hierarchical Ti_3C_2/TiO_2 composite via in situ oxidation for improved lithium-ion storage

Jianlin Zhang[1][a], Shan Wei[1][a], Qingyun Miao[a], Huihui Yue[a], Xiuxia Meng[a], Fei Wang*[a] and Naitao Yang*[a]

[a]*School of Chemistry and Chemical Engineering, Shandong University of Technology, Zibo 255049, China*

**Corresponding author: wangfei2008@sdut.edu.cn, naitaoyang@126.com*

[1]*These authors contributed equally to this work.*

1. Experimental Procedures

1.1 Synthesis of 2D few-layered $Ti_3C_2T_x$

1.0 g of commercial Ti_3AlC_2 powder (purity > 99.5%, Foshan xinxi technology Co., Ltd) as the raw material was thoroughly mixed with a prepared solution that included 1.6 g lithium fluoride (LiF, Aladdin Shanghai Co., Ltd) and 16 mL of a 12 M hydrochloric acid (HCl, Aladdin Shanghai Co., Ltd). The resulting blend was vigorously and continuously stirred at a temperature of 55°C for a period of 24 hours, resulting a dark turbid mixture. After that, the resultant mixture was washed using a 1 mol/L HCl solution three times, followed by a thorough rinse with deionized water until a pH of approximately neutral. The mixture was then redispersed in deionized water and stirred for an additional 24 hours. Following this, the dark green precipitate was exfoliated via ultrasonication for 1 hour, yielding a colloidal solution of few-layer $Ti_3C_2T_x$. The suspension was subsequently processed through vacuum freeze-drying to obtain the 2D $Ti_3C_2T_x$.

1.2 Fabrication of melamine formaldehyde spheres (MFS)

The synthesis of melamine formaldehyde spheres (MFS) is obtained through a deliberate polymerization process. Typically, 5.6 g of melamine (Macklin, China) was meticulously introduced into a solution containing 20 mL formaldehyde (TCI) and 400 mL deionized water under stirring 80°C for 20 min. Subsequently, 0.6 mL of formic acid (TCI) was incrementally added to the mixture and then stirred continuously for another 40 min. The resulting white sediment was centrifuged, washed, and vacuum-dried to obtain white solid melamine formaldehyde spheres (MFS).

1.3 Preparation of 3D porous Ti_3C_2

During the electrostatic self-assembly process, 0.6 g of the MFS was dispersed using ultrasonication in a 100 mL solution of deionized water. Thereafter, 0.2 g of the few-layed $Ti_3C_2T_x$ MXene solution was incrementally added to the mixture with concurrent vigorous stirring for 1 hour. Then, the ensuing colloidal solution was processed by centrifugation, washing, and subsequently freezing-dried to obtain a Ti_3C_2-MFS mixture. Ultimately, the dried samples underwent annealing at 550 ºC for 2h (5ºC min^{-1}) in a nitrogen atmosphere to synthesize the 3D porous Ti_3C_2.

1.4 Preparation of Ti_3C_2/TiO_2 nanocomposite

The pre-fabricated 2D few-layered $Ti_3C_2T_x$ and 3D porous Ti_3C_2 powders were thermally processed in a tubular furnace at 650 ºC for 6 h (5°C/min) in a nitrogen atmosphere (referred to as 2D Ti_3C_2/TiO_2 and 3D Ti_3C_2/TiO_2, respectively). In contrast, 2D few-layered $Ti_3C_2T_x$ and 3D porous Ti_3C_2 powder were calcined following the same temperature procedure in an air atmosphere (denoted as 2D TiO_2 and 3D TiO_2, respectively).

1.5 Structural Characterization

For the detailed characterization of the samples, scanning electron microscopy (SEM, Hitachi, S-4800) and high-resolution transmission electron microscopy (TEM, Tecnai G2 F20 S-TWIN, FEI) were meticulously employed to scrutinize the surface morphology and microstructure. X-ray diffraction (XRD) was performed to identify the crystalline phases, using a Bruker D8 X-ray diffractometer to analyze crystallographic information. Subsequently, Raman spectroscopy was conducted with a 532 nm laser on a Horiba LabRAM Aramis system to analyze the compositional analysis of the samples. Additionally, elemental valence state analysis of the synthesized samples utilized X-ray photoelectron spectroscopy (XPS, Thermo Kalpa). Furthermore, to assess the specific surface area and porosity characteristics, nitrogen adsorption-desorption isotherms were determined by a Micromeritics ASAP 2020 analyzer, applying the Brunauer-Emmett-Teller (BET) method for a comprehensive analysis.

1.6 Fabrication of the Half Cells for electrochemical characterizations

Active materials, acetylene black, and polyvinylidene fluoride (PVDF) binder (Shenzhen Kejingstar Technology Ltd., China) were combined in an 80:10:10 weight ratio to form a homogeneous mixture. This mixture was then dispersed in N-methyl-2-pyrrolidone (NMP) to create a uniform slurry, which was evenly coated onto a copper foil and dried under vacuum. The loading mass of the electrode was standardized to a range of 0.8-1.0 mg. The working electrode was integrated with a lithium foil serving as both the reference and counter electrode to form the half-cell, separated by a Celgard 2400 membrane. The electrolyte was a 1 M $LiPF_6$ in a 1:1 (v/v) mixture of ethylene carbonate (EC) and diethyl carbonate (DEC) provided from DoDoChem. The entire assembly process took place in an Ar-filled glove box (H_2O, O_2<0.1 ppm). Galvanostatic charge/discharge profiles of the battery were measured using a Neware battery testing device (CT-4008Tn Shenzhen, China) within a voltage range of 0.01 to 3.0 V vs. Li^+/Li. For a deeper analysis of the electrochemical properties, cyclic voltammetry (CV) measurements and electrochemical impedance spectroscopy (EIS)

collected using an electrochemical station (CHI660d, Shanghai Chenhua Instruments Inc., China).

The analysis of the charge storage behavior of the electrode can be based on the following formula: The relationship between peak current (i) and the sweep rate (v) followed the equation: $i = av^b$. Where a and b are the empirical parameters, the slope and cut of the linear relationship between the log i and the log v, respectively. To analyze the ratio of capacitance behavior and the diffusion process, according to the following formula: $i\ (V) = k_1v + k_2v^{1/2}$. Where k_1v represents the contribution of capacitance control and $k_2v^{1/2}$ represents the contribution of diffusion control.

The lithium-ion diffusion coefficient of the electrode material, the following equation is used:

$$D_{Li^+} = \frac{R^2T^2}{2A^2n^4F^4C^2\sigma^2}$$

Where R, T, A, n, F, C and σ are the gas constant, absolute temperature, surface area, number of electrons transferred, Faraday constant, concentration of lithium-ions in the solid and Warburg factor, which are correlative to Z':

$$Z' = R_e + R_{ct} + \sigma\omega^{-1/2}$$

Where ω is the angular frequency ($\omega = 2\pi f$).

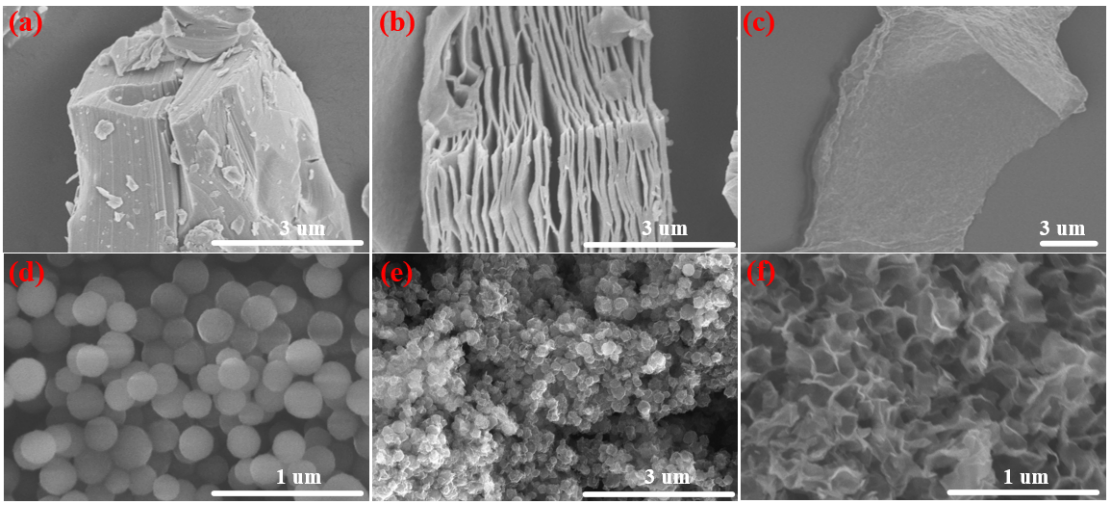

Figure S1. The SEM image of (a) Ti_3AlC_2 powder;(b) accordion-like multilayer $Ti_3C_2T_x$ MXene; (c) 2D few-layer $Ti_3C_2T_x$ MXene; (d) MFS; (e) $Ti_3C_2T_x$ MXene-MFS hybrid; (f) 3D porous Ti_3C_2.

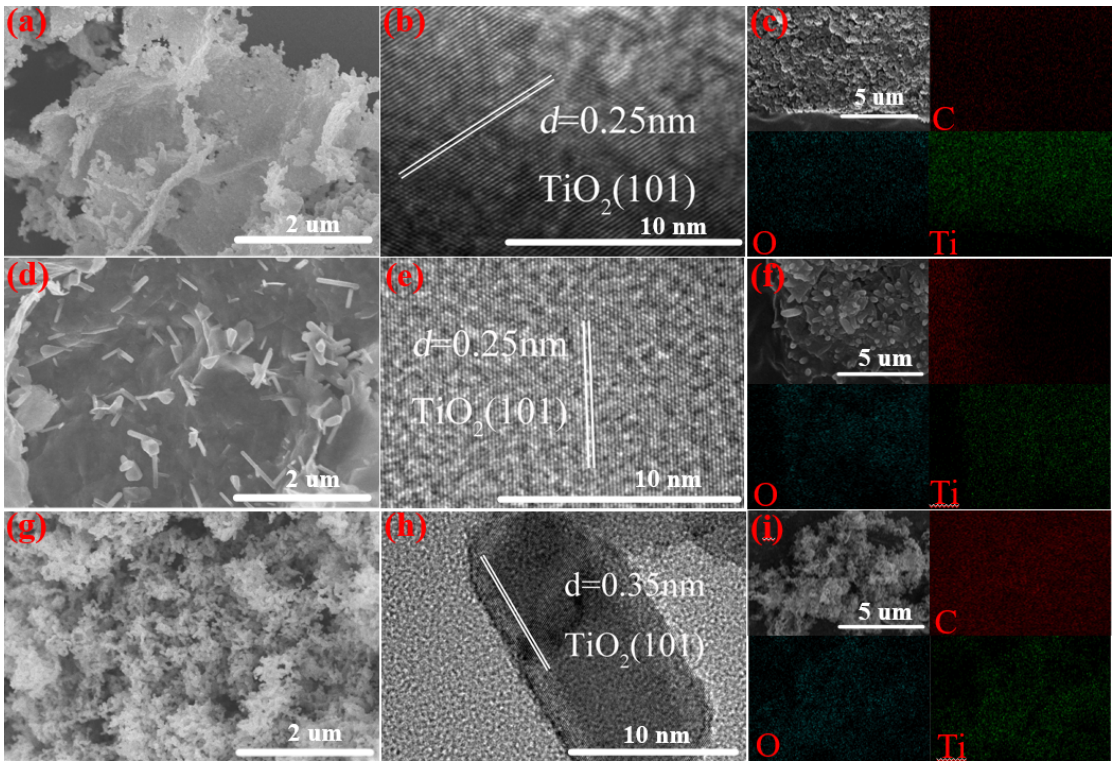

Figure S2. The 2D TiO_2 of (a) SEM image; (b) HRTEM image; (c) elemental mapping; the 2D Ti_3C_2/TiO_2 of(d) SEM image; (e) HRTEM image; (f) elemental mapping; the 3D TiO_2 of (g) SEM image; (h) HRTEM image; (i) elemental mapping.

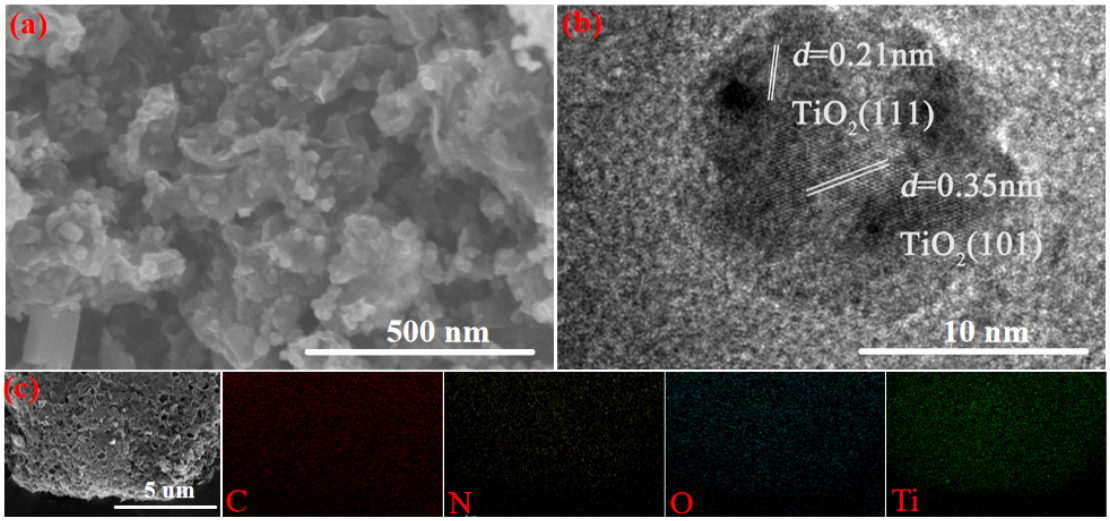

Figure S3. The 3D Ti_3C_2/TiO_2 of (a) SEM image; (b) HRTEM image; (c) elemental mapping.

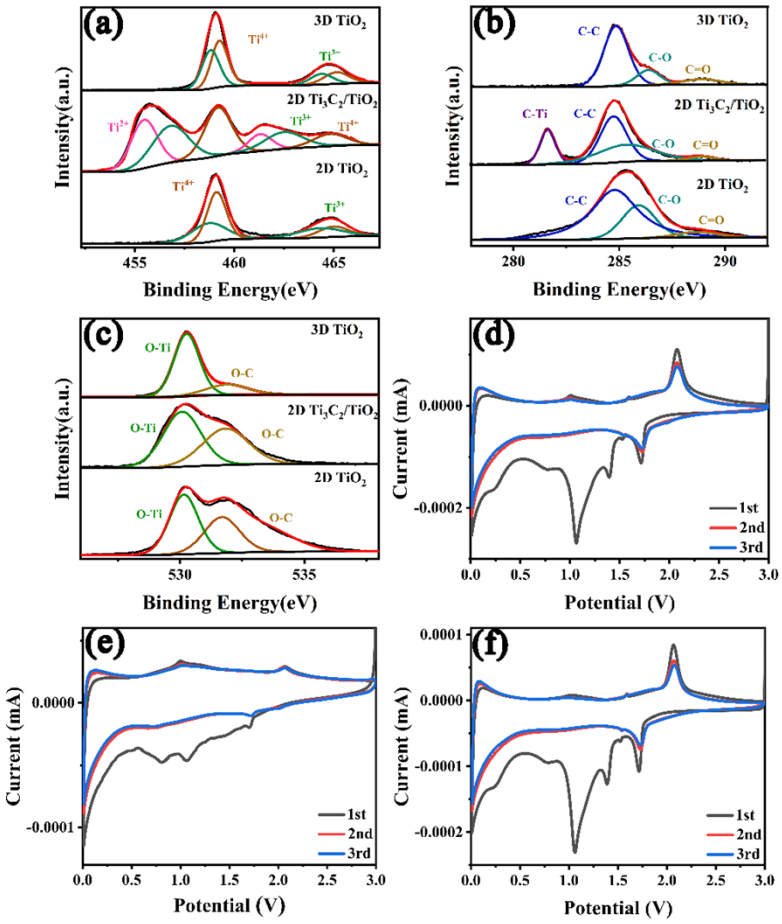

Figure S4. The XPS spectroscopy of (a) Ti2p; (b) C1s; (c) O1s; the cyclic voltammetry of (d) 2D TiO_2; (e) 2D Ti_3C_2/TiO_2; (f) 3D TiO_2.

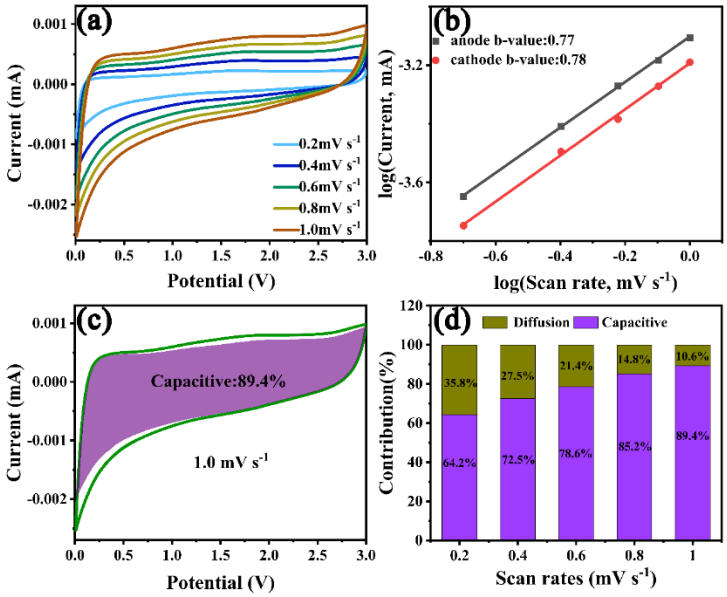

Figure S5. The 3D Ti_3C_2/TiO_2 of (a) CV curves at different scan rates; (b) log(i)-log(v) linear plots; (c) CV curve at 1.0 mV s^{-1} with shaded portion (purple area) showing the capacitive contribution; (d) Capacitive contribution at different scan rates.

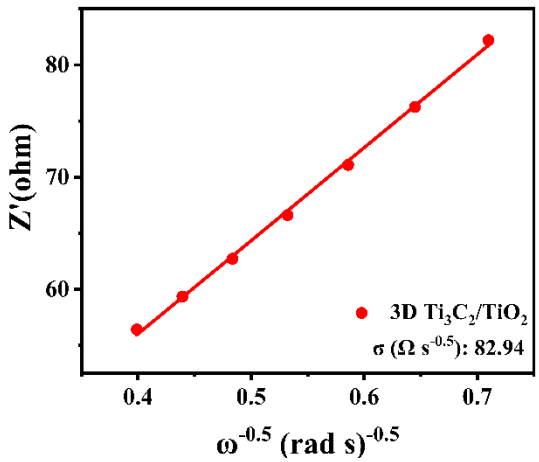

Figure S6. The relationship between Z 'and $\omega^{-0.5}$ in the low-frequency region of 3D Ti_3C_2/TiO_2.

Table S1. Comparison of electrochemical performance in this work and reported previously for TiO_2/MXene composite anodes in LIBs.

Samples	Cycling performance		References
	Current density	Capacity	
TiO_2-C hybrid	1C	155 mA h g^{-1} after 250 cycles	1
G-TiO_2 NSs	1C	161 mA h g^{-1} after 120 cycles	2
layer-stacked TiO_2	6C	107.1 mA h g^{-1} after 10000 cycles	3
TiO_2@$Ti_3C_2T_x$	0.05 A g^{-1}	80 mA h g^{-1}	4
TiO_2/Ti_3C_2 nanohybrid	2.0 A g^{-1}	202 mA h g^{-1} after 2000 cycles	5
TiO_2/MXene	0.5 A g^{-1}	209 mA h g^{-1} after 200 cycles	6
TiO_2/Ti_3C_2	1.0 A g^{-1}	141.4 mA h g^{-1} after 250 cycles	7
Ti_3C_2@TiO_2 hybrid	0.2 A g^{-1}	302 mA h g^{-1} after 500 cycles	8
2D TiO_2 nanoflakes	0.1 A g^{-1}	246.6 mA h g^{-1} after 100 cycles	9
TiO_2-Ti_3C_2 nanocomposites	0.1C	180 mA h g^{-1} after 100 cycles	10
TiO_2@$TiVCT_x$	0.1 A g^{-1}	741.2 mA h g^{-1}	11
$TiO_2/Ti_3C_2T_x$ composite	0.1 A g^{-1}	282.3 mA h g^{-1} after 200 cycles	12
3D Ti_3C_2/TiO_2 nanorod composites	1.0 A g^{-1}	384.1 mA h g^{-1} after 600 cycles	in this work

References

1 M. Naguib, O. Mashtalir, M. R. Lukatskaya, B. Dyatkin, C. Zhang, V. Presser, Y. Gogotsi and M. W. Barsoum, *Chem. Commun.*, 2014, **50**, 7420-7423.

2 S. Ding, J. S. Chen, D. Luan, F. Y. C. Boey, S. Madhavi and X. W. Lou, *Chem. Commun.*, 2011, **47**, 5780-5782.

3 H. Tang, S. Zhuang, Z. Bao, C. Lao and Y. Mei, *ChemElectroChem*, 2016, **3**, 871-876.

4 C. J. Zhang, S. J. Kim, M. Ghidiu, M.-Q. Zhao, M. W. Barsoum, V. Nicolosi and Y. Gogotsi, *Adv. Funct. Mater.*, 2016, **26**, 4143-4151.

5 C. Yang, Y. Liu, X. Sun, Y. Zhang, L. Hou, Q. Zhang and C. Yuan, *Electrochimica Acta*, 2018, **271**, 165-172.

6 Y. T. Liu, P. Zhang, N. Sun, B. Anasori, Q. Z. Zhu, H. Liu, Y. Gogotsi and B. Xu, *Adv. Mater.*, 2018, **30**, e1707334.

7 L. Jia, Y. Li, L. Su, D. Liu, Y. Fu, J. Li, X. Yan and D. He, *Chem. Select*, 2020, **5**, 3124-3129.

8 L. Li, G. Jiang, C. An, Z. Xie, Y. Wang, L. Jiao and H. Yuan, *Nanoscale*, 2020, **12**, 10369-10379.

9 Y. He and H. Li, *New. J. Chem.*, 2022, **46**, 16260-16264.

10 H. Abdurehman Tariq, U. Nisar, J. James Abraham, Z. Ahmad, S. AlQaradawi, R. Kahraman and R. A. Shakoor, *Appl Surf. Sci.*, 2022, **583**, 152441

11 K. Chen, Y. Guan, L. Tan, H. Zhu, Q. Zhang, J. Guo, Z. Dong, G. Yuan, X. Li and Y. Cong, *Appl Surf. Sci.*, 2023, **617**, 156575.

12 J. Liu, C. Du, L. Zou and P. Li, *Mater. Lett.*, 2023, **349**, 134648.